# Chirality in the Kagome Metal $CsV_3Sb_5$

H. J. Elmers[1,*] O. Tkach[1,2] Y. Lytvynenko[1,3] P. Yogi[1] M. Schmitt[4,5] D. Biswas[4] J. Liu[4] S. V. Chernov[6]
Quynh Nguyen[7] M. Hoesch[6] D. Kutnyakhov[6] N. Wind[6,8] L. Wenthaus[6] M. Scholz[6] K. Rossnagel[8,9]
A. Gloskovskii[6] C. Schlueter[6] A. Winkelmann[10] A.-A. Haghighirad[11] T.-L. Lee[4] M. Sing[5] R. Claessen[5]
M. Le Tacon[11] J. Demsar[1] G. Schönhense[1] and O. Fedchenko[1]

[1]Institut für Physik, Johannes Gutenberg-Universität, Staudingerweg 7, D-55128 Mainz, Germany
[2]Sumy State University, Kharkivska 116, 40007 Sumy, Ukraine
[3]Institute of Magnetism of the NAS and MES of Ukraine, 03142 Kyiv, Ukraine
[4]Diamond Light Source Ltd., Didcot OX11 0DE, United Kingdom
[5]Physikalisches Institut and Würzburg-Dresden Cluster of Excellence ct.qmat,
Julius-Maximilians-Universität, D-97074 Würzburg, Germany
[6]Deutsches Elektronen-Synchrotron DESY, 22607 Hamburg, Germany
[7]Linac Coherent Light Source, SLAC National Accelerator Laboratory, Menlo Park, California 94025, USA
[8]Institut für Experimentelle und Angewandte Physik, Christian-Albrechts-Universität zu Kiel, 24098 Kiel, Germany
[9]Ruprecht Haensel Laboratory, Deutsches Elektronen-Synchrotron DESY, 22607 Hamburg, Germany
[10]Academic Centre for Materials and Nanotechnology, AGH University of Krakow, 30059 Kraków, Poland
[11]Institute for Quantum Materials and Technologies, Karlsruhe Institute of Technology, 76021 Karlsruhe, Germany

Using x-ray photoelectron diffraction (XPD) and angle-resolved photoemission spectroscopy, we study photoemission intensity changes related to changes in the geometric and electronic structure in the kagome metal $CsV_3Sb_5$ upon transition to an unconventional charge density wave (CDW) state. The XPD patterns reveal the presence of a chiral atomic structure in the CDW phase. Furthermore, using circularly polarized x-rays, we have found a pronounced nontrivial circular dichroism in the angular distribution of the valence band photoemission in the CDW phase, indicating a chirality of the electronic structure. This observation is consistent with the proposed orbital loop current order. In view of a negligible spontaneous Kerr signal in recent magneto-optical studies, the results suggest an antiferromagnetic coupling of the orbital magnetic moments along the $c$ axis. While the inherent structural chirality may also induce circular dichroism, the observed asymmetry values seem to be too large in the case of the weak structural distortions caused by the CDW.

Kagome systems have recently attracted interest because of their unique electronic band structure, which exhibits delocalized electrons, Dirac points, flat bands, and multiple van Hove singularities (vHS) near the Fermi level [1–4]. The large density of states near vHSs can promote various electronic orders, such as superconductivity, chiral charge density wave (CDW), and orbital loop current order [5–8]. The vHSs in combination with flat bands can be the origin of correlated many-body ground states [9–14]. In particular, the kagome metals $AV_3Sb_5$ ($A$ = K, Rb, Cs) combine unconventional charge orders [15–21], superconductivity [22–29], lattice frustration, and non-trivial topology [30–32]. Spectroscopic evidence for topological properties and correlation effects have been provided by ARPES studies [29,33] and density functional theory [34–38]. In particular, the charge order has been related to time-reversal symmetry breaking (TRS) [16,22,30,31] or rotational symmetry breaking [17,18,21].

In the normal high temperature state, $AV_3Sb_5$ is a topological metal [29,39] with topologically protected surface states near the Fermi level [29]. In the low temperature CDW state, scanning tunneling spectroscopy (STM) [31,40] and theory [36] have suggested a chiral CDW order that breaks the time-reversal symmetry [36]. Observations of an anomalous Hall effect [32,41–43] together with muon spin relaxation [30,44] and magneto-optical Kerr effect (MOKE) studies [16,45,46] provided further evidence for the spontaneous time-reversal symmetry breaking. However, recent dedicated MOKE studies with zero-loop Sagnac interferometers [47–49] and STM [50] conclude that the occurrence of time-reversal symmetry breaking is unlikely.

Here, we use electron momentum microscopy to gain further insight into the structural and electronic chiral order in this system. The cylindrical detection geometry of momentum microscopy, which is aligned with the $c$-axis of the sample, and the fixed illumination geometry avoid

*Contact author: elmers@uni-mainz.de

misalignment artifacts [51]. Hard x-ray photoelectron diffraction (XPD) reveals a chiral order in the atomic structure in the CDW phase. On the other hand, photoelectrons excited by circularly polarized light in the soft x-ray region show spontaneous chiral symmetry breaking in the valence band states, which is particularly pronounced at certain mirror symmetry points in reciprocal space (i.e., $M$ points). We discuss time-reversal symmetry breaking or mirror symmetry breaking as possible origins for the observed effects.

The experiments were performed on single crystals of $CsV_3Sb_5$ grown by the flux method and characterized by x-ray diffraction and energy-dispersive x-ray analysis [15,52]. The $CsV_3Sb_5$ structure and the experimental geometries for the photoemission experiments are given in the Supplemental Material [53], which includes Refs. [54,54–63]. The single crystals were freshly cleaved in ultrahigh vacuum. No magnetic fields were applied before or during the experiment.

$CsV_3Sb_5$ shows a CDW reconstruction below the transition temperature ($T_{CDW} = 94$ K) [2]. To study the CDW-induced changes in the crystal structure we used core level XPD. Experiments in the hard x-ray range at 6 keV were performed at the time-of-flight momentum microscopy end station of the hard x-ray beam line P22 at PETRA III [64]. The angle of incidence was $\theta = 10°$ with respect to the sample plane and the energy resolution was set to 60 meV. XPD was performed on the Cs 4d, V 2p, and Sb 3d core levels, all of which show a pronounced XPD pattern with a sixfold symmetry.

The Cs 4d pattern [Fig. 1(a)] recorded in the high-$T$ phase shows an inner sixfold star (vertical orientation) surrounded by a ring of high intensity peaks in a straddled orientation (yellow circle). This is consistent with the pattern [Fig. 1(b)] calculated using a Bloch wave approach with the normal state crystal structure parameters determined by XRD [65,66]. Below the CDW transition, the overall appearance of the XPD pattern does not change much [Fig. 1(c)], in agreement with the Bloch wave calculation considering the $(2 \times 2 \times 4)$ reconstruction [65,66] [Fig. 1(d)]. To highlight the broken mirror symmetry (chirality) of the low-T XPD pattern we plot the difference $I(k_x, k_y) - I(-k_x, k_y)$ in Fig. 1(e). While the difference still shows a sixfold symmetry, the mirror symmetry of the XPD pattern is broken, as shown by a counterclockwise bending of the tips of the inner star in the XPD pattern. Indeed, a similar chirality shows up in the calculated XPD pattern [Fig. 1(f)] based on the low-$T$ XRD data from Refs. [65,66]. A corresponding analysis was performed for the V 2p and Sb 3d core level XPD patterns for $T < T_{CDW}$ and $T > T_{CDW}$ (see Supplemental Material [53]). These results demonstrate the structural chirality of the CDW order and imply that the domain size is larger than the x-ray footprint on the sample ($\approx 50$ μm in diameter), consistent with earlier domain mapping studies [16].



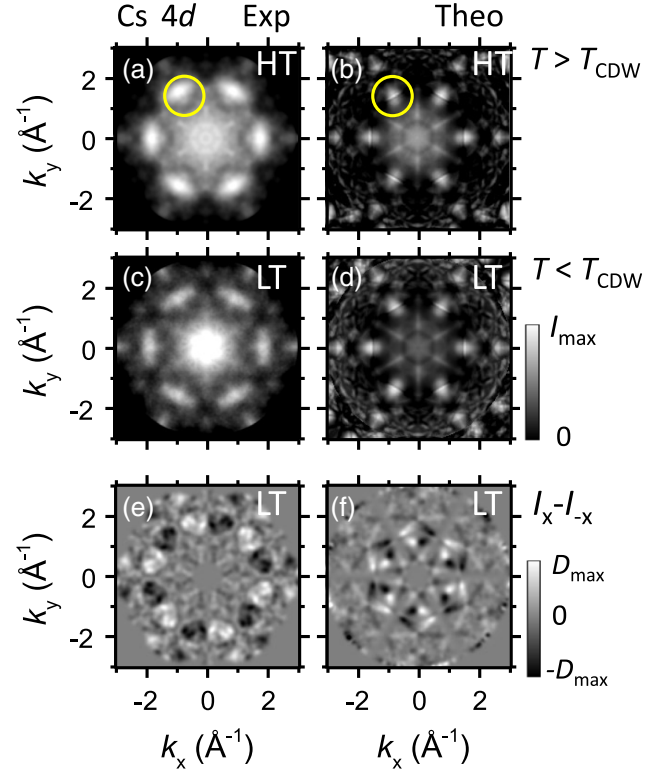FIG. 1. X-ray photoelectron diffraction of $CsV_3Sb_5$ measured at a photon energy of 6 keV for $T > T_{CDW}$ (HT, 115 K) and $T < T_{CDW}$ (LT, 30 K). Comparison of experimental (a),(c) and theoretical (b),(d) data. (e) Difference between the original data from (c) and the same data but mirrored at $k_x = 0$ to highlight the broken mirror symmetry. (f) Similar data for the calculated results (see Supplemental Material [53] for HT and other core levels).

To detect the chirality in the electronic structure valence band photoemission was performed. Circular dichroism experiments in the soft x-ray range were performed at the soft x-ray ARPES end station of Beamline I09 at Diamond Light Source, UK [67]. The angle of incidence for the circularly polarized x-rays was $\theta = 22.5°$ with respect to the sample surface, which was oriented to align the $\Gamma$-M-L plane with the incident beam. The total energy resolution was set to 50 meV. Figure 2 shows the experimental Fermi surface of $CsV_3Sb_5$ measured at the two temperatures $T_H = 115$ and $T_L = 30$ K, i.e., above and below $T_{CDW} = 94$ K. In Figs. 2(a)–2(e) we plot the photoemission intensity distribution $I(E_F, k_x, k_y)$ at the Fermi energy as a function of the parallel momentum $k_x$, $k_y$. The photon energies were varied in an interval from 210 to 250 eV, covering a perpendicular momentum range from $k_z = 11G_{001}$ to $12G_{001}$ [Figs. 2(c)–2(e)]. We observe no significant dispersion along $k_z$, indicating a two-dimensional character of the electronic states. This is in agreement with previous observations [2].

From the photoemission intensities measured with circularly polarized x-ray excitation, $I^{+/-}$, we determine the asymmetry $A^* = (I^+ - I^-)/(I^+ + I^-)$. The nonrelativistic
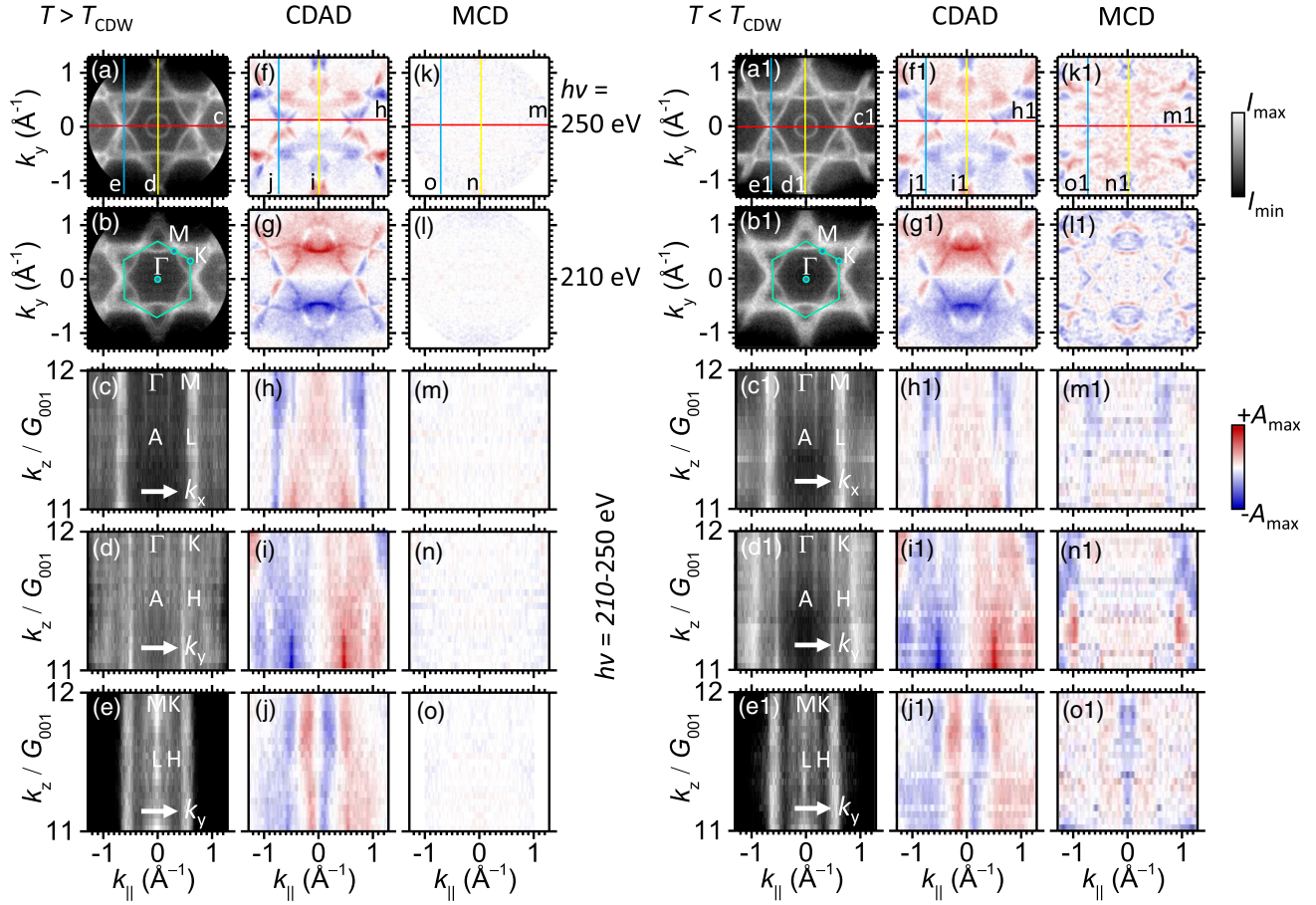
FIG. 2. (a),(b) Fermi surface of $CsV_3Sb_5$ measured at $h\nu = 250$ eV (a) and 210 eV (b) for $T > T_{CDW}$. The photon incidence is from the right. (c)–(e) Fermi surface sections in the $k_z - k_{||}$ planes (perpendicular to the surface) corresponding to the lines indicated in (a). The photon energy has been varied between 210 and 250 eV in small steps. (f)–(j) $A_{CDAD}$ in the same Fermi surface sections as in (a)–(e) [(h) shifted to $k_y > 0$ to avoid the $A_{CDAD} = 0$-line]. The maximum asymmetry of the color scale (right) is $A_{max} = 0.5$. (k)–(o) $A_{MCD}$ in the same Fermi surface sections as in (a)–(e). The maximum asymmetry of the color scale is in this case $A_{max} = 0.1$. (a1)–(o1) Similar data measured at 30 K ($T < T_{CDW}$) plotted on the same scales.

circular dichroism in the angular distribution (CDAD) is a geometric effect and it is strictly antisymmetric with respect to the photon plane of incidence, which coincides with the Γ-M-A crystal mirror plane [68]. To separate the CDAD from any other contribution, we calculate the asymmetry shown in Figs. 2(f)–2(j) as $A_{CDAD}(k_x, k_y) = (1/2)[A^*(k_x, k_y) - A^*(k_x, -k_y)]$ (see detailed discussion of the separation procedure in Ref. [69]). The maximum asymmetry is 0.5, and leads to a significant intensity redistribution when the x-ray helicity is switched. The CDAD asymmetry depends strongly on the photon energy, as can be seen by comparing Figs. 2(f) and 2(g) (see Ref. [70]). The photon energy series shows a continuous change of the asymmetry with varying $k_z$ for several electronic bands. Only the states near the M-L line show a constant asymmetry independent of the photon energy, as emphasized by the $k_z$ dependence shown in Figs. 2(h) and 2(j).

Note that at $T > T_{CDW}$, the dichroism is completely dominated by the CDAD. This can be visualized by the

complementary magnetic circular dichroism (MCD), which is symmetric with respect to the $k_y$ direction [71], $A_{MCD}(k_x, k_y) = (1/2)[A^*(k_x, k_y) + A^*(k_x, -k_y)]$, as shown in Figs. 2(k)–2(o). $A_{MCD}$ is less than 0.01 and shows no systematic variation as a function of parallel and perpendicular momentum. The lack of $A_{MCD}$ confirms the nonmagnetic character of the electronic states in $CsV_3Sb_5$ in its normal state at $T > T_{CDW}$.

At 30 K, the average photoemission intensity distribution shown in Figs. 2(a1)–2(e1) has not changed much. There are no obvious changes in the dispersion of the visible bands, only the intensity distribution near the M-L line [central line at $k_{||} = 0$ in Fig. 2(e1)] changes slightly. This observation is in agreement with previous reports using a higher energy resolution [72,73], where the CDW-induced gap opening appears near the M point. The CDW-induced band gap is discussed in the Supplemental Material [53].

The CDAD asymmetry in the CDW state [Figs. 2(f1)–2(j1)] shows a similar pattern to that observed in the normal
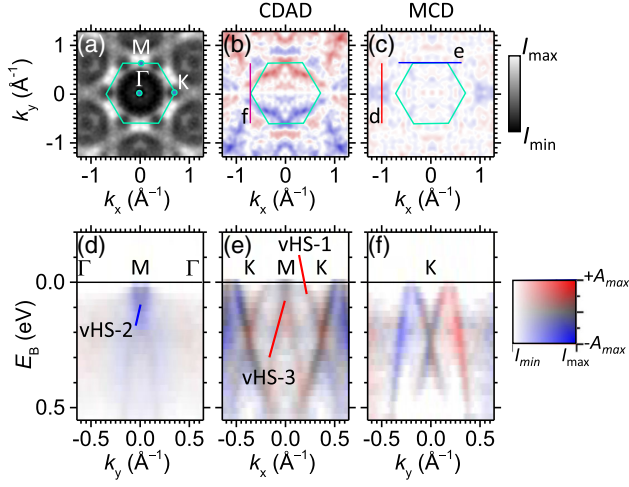
FIG. 3. (a) Fermi surface of $CsV_3Sb_5$ measured at a photon energy of 330 eV for $T < T_{CDW}$. The photon incidence is from the right. (b) CDAD texture of the Fermi surface. The maximum asymmetry of the color scale (right) is $A_{max} = 0.5$. (c) MCD asymmetry of the Fermi surface. The maximum asymmetry of the color scale (right) is $A_{max} = 0.1$. (d),(e) Band dispersion with overlaid MCD asymmetry (two-dimensional color scale on the right) along the indicated lines in (c). (f) Band dispersion with overlaid CDAD asymmetry across the $K$-point along the indicated line in (b).
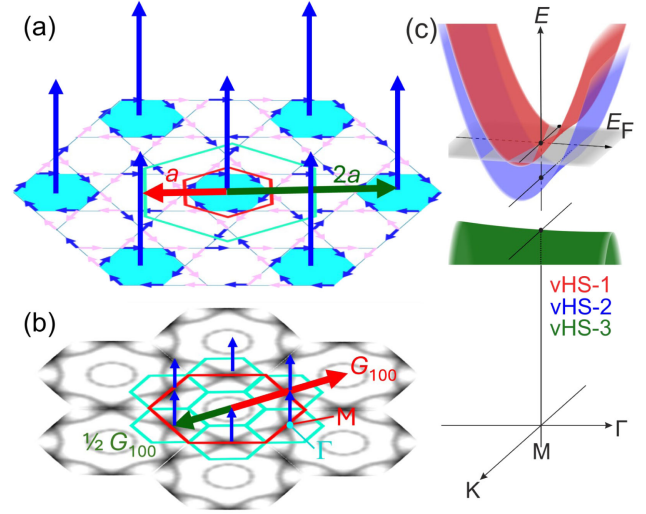


FIG. 4. (a) V-Sb plane constituting the kagome lattice. Small arrows indicate the loop current order forming a $2 \times 2$ superstructure of orbital moments (large arrows). The superstructure Wigner-Seitz cell is indicated in green and the normal state unit cell in red with corresponding unit vectors along the $a$ axis. (b) Fermi surface in reciprocal space (gray level is proportional to the measured photoemission intensity). Hexagons indicate the Brillouin zones of the normal state structure (red) and the $2 \times 2$ superstructure (green) with corresponding reciprocal lattice vectors. The blue arrows indicate the expected orbital moments near the $M$ points where the Fermi wave vector and the $\Gamma$ points of the $2 \times 2$ superstructure coincide. (c) Sketch of the first three vHSs near $E_F$.

state. The fact that no obvious CDW-induced change in CDAD is observed implies the absence of a significant change in orbital charge redistribution.

In contrast, the low-$T$ data show a significant $k_y$-symmetric $A_{MCD}$ [Figs. 2(k1)–2(o1)]. A prominent, almost $k_z$-independent, contribution appears near the $M$-$L$ line at $(k_x = \pm 0.7 \text{ Å}^{-1}, k_y = 0, k_z)$. This is unexpected for a paramagnetic system. The two $M$ points at $k_y = 0$ coincide with the antisymmetry axis of the CDAD, where the CDAD vanishes. The large asymmetry of about $-0.1$ is essentially independent of the photon energy [Figs. 2(m1) and 2(o1)]. Especially near $k_y = 0$ a pronounced nonzero $A_{MCD}$ occurs that cannot be explained by an artifact due to different sample illumination. Significant $A_{MCD}$ values also show up at $(k_x = 0, k_y = \pm 1 \text{ Å}^{-1}, k_z)$ [Fig. 2(n1)]. Here, the sign of $A_{MCD}$ changes at about $k_z = 11.5G_{001}$, which hints at additional diffraction-related asymmetries or matrix-element effects [70].

Further details of the band dispersion versus binding energy as measured at 30 and 115 K are discussed in Supplemental Material [53].

To further elucidate the CDW-induced chirality using a different experimental geometry, we performed a soft x-ray photoemission experiment with the time-of-flight momentum microscope at the soft x-ray beamline P04 at PETRA III, DESY, Germany [54], with the total energy resolution set to 34 meV. We used 330 eV x-rays (corresponding to $k_z = 13.7G_{001}$) and the same angle of incidence $\theta = 22.5°$.

In this case, however, the plane of incidence was along the $\Gamma$-$K$-$H$ plane.

Figure 3(a) shows the measured Fermi surface recorded in this configuration at 30 K. The CDAD asymmetry at the Fermi surface, Fig. 3(b) is antisymmetric with respect to the plane of incidence, with the maximum asymmetry $A_{max} \approx 0.5$ similar to the previous case. The MCD asymmetry Fig. 3(c) also shows negative values up to $-0.1$ near the $M$ point at $(k_x, k_y) = (\pm 1 \text{ Å}^{-1}, 0)$ in the adjacent Brillouin zones on the $\Gamma$-$K$ symmetry axis ($k_y = 0$ axis). The sections along $M$-$\Gamma$ [Fig. 3(d)] and $M$-$K$ [Fig. 3(e)] suggest that the negative MCD asymmetry is related to the electronlike band with a maximum binding energy of 0.1 eV at the $M$ point, which belongs to the van Hove singularity vHS-2 [see Supplemental Material for a detailed description of the vHSs [53] and Fig. 4(c)]. Bands associated with vHS-1, i.e., the flat band near the Fermi level at the $M$ point [see Fig. 3(e)], and vHS-3 (holelike band) have positive $A_{MCD}$ values. The large MCD asymmetries near the $M$ points confirm our findings obtained with the photon plane of incidence coinciding with the $\Gamma$-$M$-$A$ plane (Fig. 2).

Since the multiple vHSs with opposite mirror eigenvalues are close in energy, it has been proposed that the nearest neighbor electron repulsion favors a ground state with

coexisting loop current order and charge-bond order [74]. The loop current order imposes a time-reversal symmetry breaking in the CDW phase.

Figure 4(a) schematically shows the charge loop current as adapted from Ref. [2]. It can be visualized by alternating charge currents along the three sets of parallel lines connecting the V atom positions. Thus, the charge current vanishes when integrated over the unit cell. The ordered charge current along the V-V bonds leads to loop currents, [Fig. 4(a)], that bypass the six V atoms. The current direction of individual bonds can be either clockwise (blue arrows) or counterclockwise (pink arrows). Every second loop shows an unfrustrated loop current (shown in light blue) forming a $2 \times 2$ superlattice.

In reciprocal space, the corresponding Brillouin zone of the $2 \times 2$ structure is shown in green in Fig. 4(b). Here, some $\Gamma$ points of the superstructure Brillouin zone coincide with the $M$ points of the larger normal-state Brillouin zone [red in Fig. 4(b)]. Since the van Hove singularities near the Fermi surface are located at these $M$ points, states with finite orbital angular momentum causing a MCD are also expected at these coincidence points [blue arrows in Fig. 4(b)].

Our experimental results are thus consistent with recent reports on the anomalous Hall effect [32,41–43], observations of chiral charge order in STM studies [31] and the early magneto-optical Kerr effect studies [16,30,32,41–46], all suggesting an orbital loop-current order. On the other hand, recent dedicated polar Kerr effect measurements seem to rule out the time-reversal symmetry breaking in $CsV_3Sb_5$ [47,49]. The absence of a measurable spontaneous Kerr effect (bulk probe) [49], with strong evidence for chiral charge ordering from surface sensitive techniques such as STM [31] and the presented ARPES data, may imply an antiferromagnetic interlayer ordering of the orbital magnetic moments in $CsV_3Sb_5$. In this case, optical dichroism averaged over many atomic layers would disappear.

On the other hand, our photoelectron diffraction results at 6 keV have shown that the lattice exhibits a chiral structure in the CDW state, which is consistent with XRD data implying a stacking of different CDW patterns along the $c$ axis [65,66]. The coexistence of the star of David and inverse star of David reconstructions in the CDW state is demonstrated by XRD [39,75], nuclear quadrupole resonance (NQR) [76], and nuclear magnetic resonance (NMR) [77] measurements. Such structural chirality may also induce the observed valence-band MCD effect, which is in this case better described as an intrinsic instead of a magnetic circular dichroism [78]. In fact, a three-dimensional structural and electronic chirality of the helix-type without time-reversal symmetry breaking would also be consistent with our experimental results. The observed asymmetry values of the order of 0.1 are, however, much larger than previously assumed for the natural circular dichroism.

[1] C. Guo, M. R. van Delft, M. Gutierrez-Amigo, D. Chen, C. Putzke, G. Wagner, M. H. Fischer, T. Neupert, I. Errea, M. G. Vergniory, S. Wiedmann, C. Felser, and P. J. W. Moll, npj Quantum Mater. **9**, 20 (2024).

[2] Y. Hu, X. Wu, A. P. Schnyder, and M. Shi, npj Quantum Mater. **8**, 67 (2023).

[3] M. Kang, S. Fang, J.-K. Kim, B. R. Ortiz, S. H. Ryu, J. Kim, J. Yoo, G. Sangiovanni, D. Di Sante, B.-G. Park, C. Jozwiak, A. Bostwick, E. Rotenberg, E. Kaxiras, S. D. Wilson, J.-H. Park, and R. Comin, Nat. Phys. **18**, 301 (2022).

[4] M. Sato and Y. Ando, Rep. Prog. Phys. **80**, 076501 (2017).

[5] Y. Xing, S. Bae, E. Ritz, F. Yang, T. Birol, A. N. Capa Salinas, B. R. Ortiz, S. D. Wilson, Z. Wang, R. M. Fernandes, and V. Madhavan, Nature (London) **631**, 60 (2024).

[6] G. Xu, B. Lian, and S.-C. Zhang, Phys. Rev. Lett. **115**, 186802 (2015).

[7] H.-M. Guo and M. Franz, Phys. Rev. B **80**, 113102 (2009).

[8] E. Tang, J.-W. Mei, and X.-G. Wen, Phys. Rev. Lett. **106**, 236802 (2011).

[9] W.-S. Wang, Z.-Z. Li, Y.-Y. Xiang, and Q.-H. Wang, Phys. Rev. B **87**, 115135 (2013).

[10] M. L. Kiesel, C. Platt, and R. Thomale, Phys. Rev. Lett. **110**, 126405 (2013).

[11] M. L. Kiesel and R. Thomale, Phys. Rev. B **86**, 121105(R) (2012).

[12] S.-L. Yu and J.-X. Li, Phys. Rev. B **85**, 144402 (2012).

[13] A. Mielke, J. Phys. A **25**, 4335 (1992).

[14] S. Vonsovsky and M. Katsnelson, Physica (Amsterdam) **159B**, 61 (1989).

[15] M. Frachet, L. Wang, W. Xia, Y. Guo, M. He, N. Maraytta, R. Heid, A.-A. Haghighirad, M. Merz, C. Meingast, and F. Hardy, Phys. Rev. Lett. **132**, 186001 (2024).

[16] Y. Xu, Z. Ni, Y. Liu, B. R. Ortiz, Q. Deng, S. D. Wilson, B. Yan, L. Balents, and L. Wu, Nat. Phys. **18**, 1470 (2022).

[17] L. Nie *et al.*, Nature (London) **604**, 59 (2022).

[18] H. Zhao, H. Li, B. R. Ortiz, S. M. L. Teicher, T. Park, M. Ye, Z. Wang, L. Balents, S. D. Wilson, and I. Zeljkovic, Nature (London) **599**, 216 (2021).

[19] H. Li *et al.*, Phys. Rev. X **11**, 031050 (2021).

[20] Z. Liang, X. Hou, F. Zhang, W. Ma, P. Wu, Z. Zhang, F. Yu, J.-J. Ying, K. Jiang, L. Shan, Z. Wang, and X.-H. Chen, Phys. Rev. X **11**, 031026 (2021).

[21] H. Chen *et al.*, Nature (London) **599**, 222 (2021).

[22] Z. Guguchia *et al.*, Nat. Commun. **14**, 153 (2023).

[23] K. Jiang, T. Wu, J.-X. Yin, Z. Wang, M. Z. Hasan, S. D. Wilson, X. Chen, and J. Hu, Natl. Sci. Rev. **10**, nwac199 (2022).

[24] Z. Zhang, Z. Chen, Y. Zhou, Y. Yuan, S. Wang, J. Wang, H. Yang, C. An, L. Zhang, X. Zhu, Y. Zhou, X. Chen, J. Zhou, and Z. Yang, Phys. Rev. B **103**, 224513 (2021).

[25] T. Neupert, M. M. Denner, J.-X. Yin, R. Thomale, and M. Z. Hasan, Nat. Phys. **18**, 137 (2021).

[26] K. Y. Chen, N. N. Wang, Q. W. Yin, Y. H. Gu, K. Jiang, Z. J. Tu, C. S. Gong, Y. Uwatoko, J. Sun, H. C. Lei, J. P. Hu, and J.-G. Cheng, Phys. Rev. Lett. **126**, 247001 (2021).

[27] X. Chen, X. Zhan, X. Wang, J. Deng, X.-B. Liu, X. Chen, J.-G. Guo, and X. Chen, Chin. Phys. Lett. **38**, 057402 (2021).

[28] H. Tan, Y. Liu, Z. Wang, and B. Yan, Phys. Rev. Lett. **127**, 046401 (2021).

[29] B. R. Ortiz, S. M. Teicher, Y. Hu, J. L. Zuo, P. M. Sarte, E. C. Schueller, A. M. Abeykoon, M. J. Krogstad, S. Rosenkranz, R. Osborn, R. Seshadri, L. Balents, J. He, and S. D. Wilson, Phys. Rev. Lett. **125**, 247002 (2020).

[30] C. Mielke *et al.*, Nature (London) **602**, 245 (2022).

[31] Y.-X. Jiang *et al.*, Nat. Mater. **20**, 1353 (2021).

[32] S.-Y. Yang, Y. Wang, B. R. Ortiz, D. Liu, J. Gayles, E. Derunova, R. Gonzalez-Hernandez, L. Šmejkal, Y. Chen, S. S. P. Parkin, S. D. Wilson, E. S. Toberer, T. McQueen, and M. N. Ali, Sci. Adv. **6**, eabb6003 (2020).

[33] Y. Hu, S. M. Teicher, B. R. Ortiz, Y. Luo, S. Peng, L. Huai, J. Ma, N. C. Plumb, S. D. Wilson, J. He, and M. Shi, Sci. Bull. **67**, 495 (2022).

[34] Y.-P. Lin and R. M. Nandkishore, Phys. Rev. B **104**, 045122 (2021).

[35] T. Park, M. Ye, and L. Balents, Phys. Rev. B **104**, 035142 (2021).

[36] X. Feng, K. Jiang, Z. Wang, and J. Hu, Sci. Bull. **66**, 1384 (2021).

[37] X. Wu, T. Schwemmer, T. Müller, A. Consiglio, G. Sangiovanni, D. Di Sante, Y. Iqbal, W. Hanke, A. P. Schnyder, M. M. Denner, M. H. Fischer, T. Neupert, and R. Thomale, Phys. Rev. Lett. **127**, 177001 (2021).

[38] M. M. Denner, R. Thomale, and T. Neupert, Phys. Rev. Lett. **127**, 217601 (2021).

[39] B. R. Ortiz, P. M. Sarte, E. M. Kenney, M. J. Graf, S. M. L. Teicher, R. Seshadri, and S. D. Wilson, Phys. Rev. Mater. **5**, 034801 (2021).

[40] Z. Wang *et al.*, Phys. Rev. B **104**, 075148 (2021).

[41] X. Wei, C. Tian, H. Cui, Y. Zhai, Y. Li, S. Liu, Y. Song, Y. Feng, M. Huang, Z. Wang, Y. Liu, Q. Xiong, Y. Yao, X. C. Xie, and J.-H. Chen, Nat. Commun. **15**, 5038 (2024).

[42] X. Zhou, H. Liu, W. Wu, K. Jiang, Y. Shi, Z. Li, Y. Sui, J. Hu, and J. Luo, Phys. Rev. B **105**, 205104 (2022).

[43] F. H. Yu, T. Wu, Z. Y. Wang, B. Lei, W. Z. Zhuo, J. J. Ying, and X. H. Chen, Phys. Rev. B **104**, L041103 (2021).

[44] R. Khasanov, D. Das, R. Gupta, C. Mielke, M. Elender, Q. Yin, Z. Tu, C. Gong, H. Lei, E. T. Ritz, R. M. Fernandes, T. Birol, Z. Guguchia, and H. Luetkens, Phys. Rev. Res. **4**, 023244 (2022).

[45] Y. Hu, S. Yamane, G. Mattoni, K. Yada, K. Obata, Y. Li, Y. Yao, Z. Wang, J. Wang, C. Farhang, J. Xia, Y. Maeno, and S. Yonezawa, arXiv:2208.08036v2.

[46] Q. Wu, Z. X. Wang, Q. M. Liu, R. S. Li, S. X. Xu, Q. W. Yin, C. S. Gong, Z. J. Tu, H. C. Lei, T. Dong, and N. L. Wang, Phys. Rev. B **106**, 205109 (2022).

[47] C. Farhang, J. Wang, B. R. Ortiz, S. D. Wilson, and J. Xia, Nat. Commun. **14**, 5326 (2023).

[48] J. Wang, C. Farhang, B. R. Ortiz, S. D. Wilson, and J. Xia, Phys. Rev. Mater. **8**, 014202 (2024).

[49] D. R. Saykin, C. Farhang, E. D. Kountz, D. Chen, B. R. Ortiz, C. Shekhar, C. Felser, S. D. Wilson, R. Thomale, J. Xia, and A. Kapitulnik, Phys. Rev. Lett. **131**, 016901 (2023).

[50] H. Li, S. Wan, H. Li, Q. Li, Q. Gu, H. Yang, Y. Li, Z. Wang, Y. Yao, and H.-H. Wen, Phys. Rev. B **105**, 045102 (2022).

[51] K. Medjanik, O. Fedchenko, S. Chernov, D. Kutnyakhov, M. Ellguth, A. Oelsner, B. Schcönhense, T. R. F. Peixoto, P. Lutz, C.-H. Min, F. Reinert, S. Däster, Y. Acremann, J. Viefhaus, W. Wurth, H. J. Elmers, and G. Schönhense, Nat. Mater. **16**, 615 (2017).

[52] F. Stier, A. A. Haghighirad, G. Garbarino, S. Mishra, N. Stilkerich, D. Chen, C. Shekhar, T. Lacmann, C. Felser, T. Ritschel, J. Geck, and M. L. Tacon, Phys. Rev. Lett. **133**, 236503 (2024).

[53] See Supplemental Material at http://link.aps.org/supplemental/10.1103/PhysRevLett.134.096401 for additional XPD data on V $2p$ and Sb $3d$ core levels, details on the electronic band dispersion, and the discussion of CDW induced changes in the electronic structure near the $M$ point of $CsV_3Sb_5$.

[54] O. Tkach *et al.*, arXiv:2401.10084v2.

[55] O. Tkach *et al.*, Ultramicroscopy **250**, 113750 (2023).

[56] T.-P. Vo, O. Tkach, S. Tricot, D. Sébilleau, A. Winkelmann, O. Fedchenko, Y. Lytvynenko, D. Vasilyev, H.-J. Elmers, G. Schönhense, and J. Minár, AIP Conf. Proc. **3251**, 020005 (2024).

[57] W. Wu *et al.*, Nat. Commun. **15**, 2313 (2024).

[58] Y. Hu, X. Wu, B. R. Ortiz, S. Ju, X. Han, J. Ma, N. C. Plumb, M. Radovic, R. Thomale, S. D. Wilson, A. P. Schnyder, and M. Shi, Nat. Commun. **13**, 2220 (2022).

[59] Y. Hu, X. Wu, B. R. Ortiz, X. Han, N. C. Plumb, S. D. Wilson, A. P. Schnyder, and M. Shi, Phys. Rev. B **106**, L241106 (2022).

[60] Y. Luo *et al.*, Phys. Rev. B **105**, L241111 (2022).

[61] H. Luo *et al.*, Nat. Commun. **13**, 273 (2022).

[62] R. Lou, A. Fedorov, Q. Yin, A. Kuibarov, Z. Tu, C. Gong, E. F. Schwier, B. Büchner, H. Lei, and S. Borisenko, Phys. Rev. Lett. **128**, 036402 (2022).

[63] Z. Jiang, H. Ma, W. Xia, Z. Liu, Q. Xiao, Z. Liu, Y. Yang, J. Ding, Z. Huang, J. Liu, Y. Qiao, J. Liu, Y. Peng, S. Cho, Y. Guo, J. Liu, and D. Shen, Nano Lett. **23**, 5625 (2023).

[64] C. Schlueter, A. Gloskovskii, K. Ederer, I. Schostak, S. Piec, I. Sarkar, Y. Matveyev, P. Lömker, M. Sing, R. Claessen, C. Wiemann, C. M. Schneider, K. Medjanik, G. Schönhense, P. Amann, A. Nilsson, and W. Drube, AIP Conf. Proc. **2054**, 040010 (2019).

[65] L. Kautzsch, B. R. Ortiz, K. Mallayya, J. Plumb, G. Pokharel, J. P. C. Ruff, Z. Islam, E.-A. Kim, R. Seshadri, and S. D. Wilson, Phys. Rev. Mater. **7**, 024806 (2023).

[66] B. R. Ortiz, S. M. L. Teicher, L. Kautzsch, P. M. Sarte, N. Ratcliff, J. Harter, J. P. C. Ruff, R. Seshadri, and S. D. Wilson, Phys. Rev. X **11**, 041030 (2021).

[67] M. Schmitt, D. Biswas, O. Tkach, O. Fedchenko, J. Liu, H.-J. Elmers, M. Sing, R. Claessen, T.-L. Lee, and G. Schönhense, arXiv:2406.00771v1.

[68] C. Westphal, J. Bansmann, M. Getzlaff, and G. Schönhense, Phys. Rev. Lett. **63**, 151 (1989).

[69] O. Fedchenko *et al.*, Sci. Adv. **10**, eadj4883 (2024).

[70] O. Fedchenko, K. Medjanik, S. Chernov, D. Kutnyakhov, M. Ellguth, A. Oelsner, B. Schönhense, T. R. F. Peixoto, P. Lutz, C.-H. Min, F. Reinert, S. Däster, Y. Acremann, J. Viefhaus, W. Wurth, J. Braun, J. Minár, H. Ebert, H. J. Elmers, and G. Schönhense, New J. Phys. **21**, 013017 (2019).

[71] J. Bansmann, C. Westphal, M. Getzlaff, F. Fegel, and G. Schönhense, J. Magn. Magn. Mater. **104–107**, 1691 (1992).

[72] K. Nakayama, Y. Li, T. Kato, M. Liu, Z. Wang, T. Takahashi, Y. Yao, and T. Sato, Phys. Rev. B **104**, L161112 (2021).

[73] D. Azoury, A. von Hoegen, Y. Su, K. H. Oh, T. Holder, H. Tan, B. R. Ortiz, A. Capa Salinas, S. D. Wilson, B. Yan, and N. Gedik, Proc. Natl. Acad. Sci. U.S.A. **120**, e2308588120 (2023).

[74] H. Li, Y. B. Kim, and H.-Y. Kee, Phys. Rev. Lett. **132**, 146501 (2024).

[75] Q. Xiao, Y. Lin, Q. Li, X. Zheng, S. Francoual, C. Plueckthun, W. Xia, Q. Qiu, S. Zhang, Y. Guo, J. Feng, and Y. Peng, Phys. Rev. Res. **5**, L012032 (2023).

[76] X. Y. Feng, Z. Zhao, J. Luo, J. Yang, A. F. Fang, H. T. Yang, H. J. Gao, R. Zhou, and G.-q. Zheng, npj Quantum Mater. **8**, 23 (2023).

[77] J. Frassineti, P. Bonfà, G. Allodi, E. Garcia, R. Cong, B. R. Ortiz, S. D. Wilson, R. De Renzi, V. F. Mitrović, and S. Sanna, Phys. Rev. Res. **5**, L012017 (2023).

[78] S. S. Brinkman, X. L. Tan, B. Brekke, A. C. Mathisen, O. Finnseth, R. J. Schenk, K. Hagiwara, M.-J. Huang, J. Buck, M. Kallane, M. Hoesch, K. Rossnagel, K.-H. Ou Yang, M.-T. Lin, G.-J. Shu, Y.-J. Chen, C. Tusche, and H. Bentmann, Phys. Rev. Lett. **132**, 196402 (2024).